Observed and modeled bio-optical, bioluminescent, and physical properties during a coastal upwelling event in Monterey Bay, California

Igor Shulman,[1] Mark A. Moline,[2] Bradley Penta,[1] Stephanie Anderson,[1] Matthew Oliver,[3] and Steven H. D. Haddock[4]

Received 14 July 2010; revised 8 November 2010; accepted 23 November 2010; published 27 January 2011.

[1] During spring and summer time, coastal upwelling influences circulation and ecosystem dynamics of the Monterey Bay, California, which is recognized as a National Marine Sanctuary. Observations of physical, bio-optical properties (including bioluminescence) together with results from dynamical biochemical and bioluminescence models are used to interpret the development of the upwelling event during August 2003 in Monterey Bay, California. Observations and the biochemical model show the development of a phytoplankton bloom in the southern portion of Monterey Bay. Model results show an increase of nutrients in the southern portion of the bay, where nutrient-rich water masses are brought in by the southward flow and cyclonic circulation inside the bay. This increase in nutrients together with the sluggish circulation in the southern portion of the bay provides favorable conditions for phytoplankton growth. Our observations and models suggest that with the development of upwelling the offshore water masses with the subsurface layer of bioluminescent zooplankton were replaced by water masses advected from the northern coast of the bay with a relatively high presence of mostly nonbioluminescent phytoplankton. Inshore observations from autonomous underwater vehicles (AUVs) show consistent coincidence of chlorophyll, backscatter, and bioluminescence maxima during upwelling development. Offshore AUV observations (taken at the entrance to the bay) show a deeper bioluminescence maximum below the surface layers of high chlorophyll and backscatter values during the earlier stages of upwelling development. Later, the observed deep offshore bioluminescence maximum disappeared and became a shallower and much weaker signal, coinciding with high chlorophyll and backscatter values offshore. Based on the biochemical and bioluminescence models, a methodology for estimating the nighttime water-leaving radiance due to stimulated bioluminescence is demonstrated and evaluated.

Citation: Shulman, I., M. A. Moline, B. Penta, S. Anderson, M. Oliver, and S. H. D. Haddock (2011), Observed and modeled bio-optical, bioluminescent, and physical properties during a coastal upwelling event in Monterey Bay, California, *J. Geophys. Res.*, *116*, C01018, doi:10.1029/2010JC006525.

1. Introduction

[2] A multi-institution, multidisciplinary Autonomous Ocean Sampling Network field experiment (called AOSN II) was conducted in the Monterey Bay, California, during August and September 2003 [*Ramp et al.*, 2009]. The Monterey Bay represented an attractive site for the experiment due to the availability of an already existing observing system including the established network of HF radars, semipermanent moored surface buoys and communications infrastructure. During northwesterly, upwelling favorable winds, the mesoscale and large-scale features in and around the Monterey Bay are mostly determined by the interaction between upwelling filaments formed at headlands to the north (Pt. Año Nuevo, Figure 1) and to the south of the Bay (Pt. Sur) and by the California Current system offshore of the Bay [*Rosenfeld et al.*, 1994]. Wind-driven upwelling of nutrient-rich water supports high levels of phytoplankton productivity in Monterey Bay [*Pennington and Chavez*, 2000; *Ryan et al.*, 2005]. Late stage phytoplankton blooms yield an accumulation of autotrophic dinoflagellates that include bioluminescent species [*Haddock et al.*, 2010; *Moline et al.*, 2009].

[1] Oceanography Division, Naval Research Laboratory, Stennis Space Center, Mississippi, USA.
[2] Center for Marine and Coastal Sciences, Biological Sciences Department, California Polytechnic State University, San Luis Obispo, California, USA.
[3] College of Marine and Earth Sciences, University of Delaware, Lewes, Delaware, USA.
[4] Monterey Bay Aquarium Research Institute, Moss Landing, California, USA.

0148-0227/11/2010JC006525

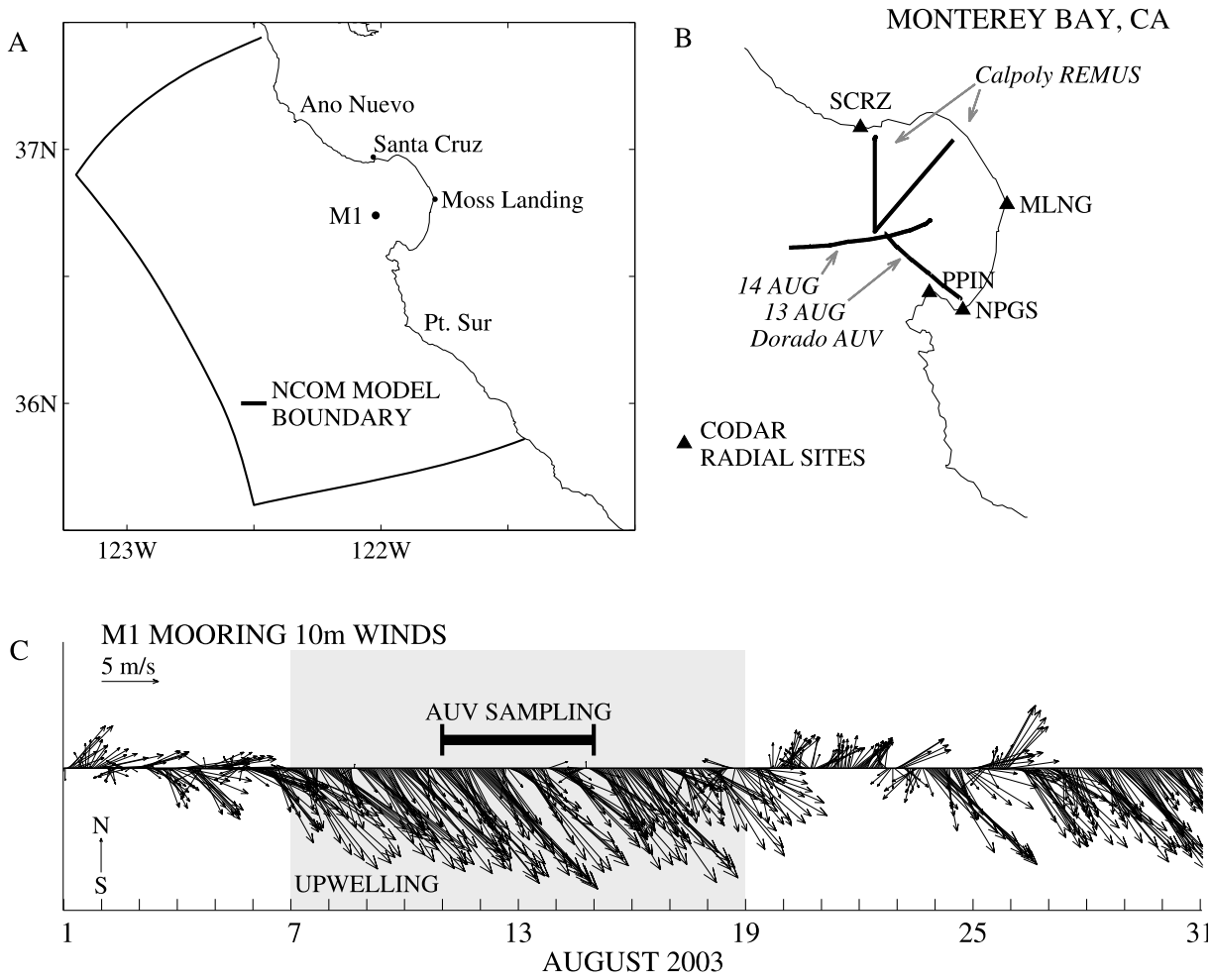

Figure 1. (a) The NCOM ICON model domain (bounded by solid black line) and M1 mooring location. (b) Locations of HF radar sites; V-shaped transect of CalPoly AUV REMUS and sections sampled by AUV DORADO. (c) Observed wind velocities at M1 during August 2003.

[3] One objective of the 2003 experiment was to learn how to apply new tools, technologies, and analysis techniques to adaptively sample the coastal ocean. Another objective was to use the gathered information to develop accurate forecasts of the bay-scale patterns of physical and biological fields, including bioluminescence [*Ramp et al.*, 2009; *Haddock et al.*, 2010; *Moline et al.*, 2005, 2009; *Shulman et al.*, 2005]. For this reason, the field program included an extensive sampling of the bay and surrounding areas with a fleet of underwater gliders, propeller-driven autonomous underwater vehicles (AUVs), a low-flying aircraft and HF radars in addition to moorings, ships, and other more traditional observational techniques (see also special issue of *Deep Sea Research Part II*, *56*, pp. 61–260, 2009).

[4] Modeling of physical conditions during the experiment was presented by *Shulman et al.* [2009, 2010]. The model (based on the Navy Coastal Ocean Model (NCOM)) was able to reproduce many observed circulation features of upwelling and relaxation events of August 2003. The physical model is coupled to the biochemical submodel of *Chai et al.* [2002]. Predictions from the physical model are also used to simulate changes in the bioluminescence intensity in accordance with methodology outlined by *Shulman et al.* [2003, 2005].

[5] The primary objective of the present study is to describe and provide the interpretation of the upwelling development during the experiment. For this reason, observations of physical, bio-optical properties (including bioluminescence) together with results from physical, biochemical and bioluminescence models are used to achieve this goal. Also, biochemical and bioluminescence dynamical models are combined together to demonstrate predictions of the nighttime water-leaving radiance due to stimulated subsurface bioluminescence.

[6] The structure of the paper is as follows: Section 2 describes observations and models. Analysis of observed and modeled bio-optical, physical properties during the upwelling event is presented in section 3. Section 4 is devoted

to the bioluminescence and the nighttime water-leaving radiance modeling. Conclusions are presented in section 5.

2. Methods

2.1. Observations

[7] Observations of winds and water velocity from the Monterey Bay Aquarium Research Institute (MBARI) surface mooring M1 (36.74°N, 122.02°W) are used in this study (Figure 1).

[8] During the 2003 field program, the mooring had a downward looking RD Instruments Inc. 75 KHz Acoustic Doppler Current Profiler (ADCP) which was set up to sample currents every 15 min. In 60 8 m bins up to 500 m depth (the first bin at 16 m depth). Surface wind speed and direction were measured by a RM Young model 05103 wind monitor.

[9] Surface current observations used in this study were derived from a network of SeaSonde-type HF radar instruments deployed in the Monterey Bay region. These instruments exploit information in the radio wave backscatter from the ocean surface to infer movement of the near surface water. Each individual SeaSonde instrument provides a distribution of "radial" velocity observations each hour on a polar coordinate grid centered on the radar site. Vector currents were estimated on a Cartesian grid with a horizontal resolution of 3 km by computing the best fit vector velocity components using all radial velocity observations within a radius of 3 km for each grid point each hour [*Paduan and Shulman*, 2004]. During the AOSN II experiment, surface currents were estimated based on input from four HF radar sites (Figure 1): Santa Cruz (SCRZ), Moss Landing (MLNG), The Naval Postgraduate School (NPGS) and the Point Pinos (PPIN).

[10] The goal of AUVs surveys was sampling of bioluminescence (BL). BL was measured using two MBBP series custom bathyphotometers developed at University of California Santa Barbara. Bathyphotometers were mounted on a CalPoly AUV (Remote Environmental Monitoring Units (REMUS)) [*Moline et al.*, 2005] and a larger MBARI DORADO AUV [*Haddock et al.*, 2010]. The bioluminescence bathyphotometer [*Herren et al.*, 2005] pumps water into a 0.5 L sample chamber at a rate of 0.35–0.4 L/s. Flow rate, temperature, and light levels (photon flux, assuming isotropic emission) are measured in the sample chamber. The instrument is calibrated both radiometrically by a known light source, and biologically by insertion of a known concentration of dinoflagellates. With the bathyphotometer, we capture a repeatable and representative fraction of the bioluminescence present in the environment. The CalPoly AUV conducted surveys along a V-shaped transect in the northern half of the Monterey Bay (Figure 1b). These operations began near Santa Cruz, ran out to MBARI surface buoy M1, then returned back to shore. These REMUS runs collected data between 2100 and 0400 LT each night on 10–18 August 2003. The vehicle followed a sawtooth pattern to 40 m depth sampling with a CTD, transmissometer, fluorometer, and ADCP in addition to a bioluminescence. The DORADO AUV sections are shown on Figure 1. Instruments on board included a CTD, fluorometer, oxygen and nitrate sensors, bioluminescence, and ADCP.

2.2. Models

[11] The Monterey Bay model (called the NCOM ICON) consists of the physical model [*Shulman et al.*, 2007], which is coupled to the biochemical model [*Chai et al.*, 2002]. The physical model of the Monterey Bay is based on the NCOM model, which is a primitive equation, 3-D, hydrostatic model. It uses the Mellor-Yamada level 2.5 turbulence closure scheme, and the Smagorinsky formulation for horizontal mixing [*Martin*, 2000]. The biochemical model of the NCOM ICON simulates dynamics of two sizes of phytoplankton, small phytoplankton cells (<5 μm in diameter) and diatoms, two zooplankton grazers, nitrate, silicate, ammonium, and two detritus pools [*Chai et al.*, 2002].

[12] The NCOM ICON model is set up on a curvilinear orthogonal grid with resolution ranging from 1 to 4 km. The model domain is shown on Figure 1. The model is forced with surface fluxes from the Coupled Ocean and Atmospheric Mesoscale Prediction System (COAMPS) [*Doyle et al.*, 2009] at 3 km horizontal resolution. The 3 km resolution COAMPS grid mesh is centered over Central California and the Monterey Bay. Phytoplankton photosynthesis in the biochemical model is driven by Photosynthetically Active Radiation (PAR), which is estimated based on the shortwave radiation flux from the COAMPS model. The *Penta et al.* [2008] scheme is used for PAR attenuation with depth.

[13] The NCOM ICON model uses the Navy Coupled Ocean Data Assimilation (NCODA) system [*Cummings*, 2005] for the assimilation of the temperature and salinity data from different observational platforms. The NCODA is a fully 3-D multivariate optimum interpolation system. Assimilation of temperature and salinity data is performed every 12 h (assimilation cycle). Differences between the NCODA analysis and the model forecast are uniformly added to the model temperature and salinity fields over the assimilation cycle. The evaluation of the NCOM ICON model predictions are presented by *Shulman et al.* [2007, 2009, 2010].

[14] Open boundary conditions for the NCOM ICON are derived from the regional model of the California Current (NCOM CCS) [*Shulman et al.*, 2007]. The NCOM CCS has a horizontal resolution of about 9 km and, the model is forced with atmospheric products derived from the COAMPS [*Doyle et al.*, 2009].

[15] Open boundary conditions for the regional NCOM CCS model are derived from the NCOM global model [*Rhodes et al.*, 2002; *Barron et al.*, 2004], which has 1/8° horizontal resolution. The model assimilates satellite-derived sea surface height (SSH) and sea surface temperature (SST) data via synthetic temperature and salinity profiles derived from the Modular Ocean Data Assimilation System (MODAS) [*Fox et al.*, 2002], and uses atmospheric forcing from the Navy Global Atmospheric Prediction System (NOGAPS) [*Rosmond et al.*, 2002].

[16] The bioluminescence model (BL model) is based on BL predictions with an advection-diffusion-reaction model (ADR), with velocities and diffusivities taken from the NCOM ICON model [*Shulman et al.*, 2005, 2003]. The BL model consists of dynamical initialization of the ADR model by assimilating available BL observations, and forecasting BL intensity with the ADR model. There is no modeling of sources and sinks of BL intensity due to biological interactions, nor modeling of behavioral dynamics

of bioluminescent organisms (for example vertical migration of dinoflagellates).

3. Bio-Optical and Physical Properties During the Upwelling Event

[17] In accordance with the observed wind velocity at the mooring M1, AUVs REMUS and DORADO surveys were conducted during the extended upwelling event of 7–19 August (Figure 1). The spatial distribution of the HF radar derived surface currents and the subsurface profiles of northward and eastward velocity components at mooring M1 are shown on Figure 2. Both surface and subsurface currents are averaged over 3 days of upwelling (15–17 August). Figure 2 indicates that during the upwelling event, there was a development of strong, wide southward flow at the surface, which extends up to 150m depth (Figure 2, negative values of V component of the mooring M1 currents indicate southward flow). This southward flow separates a pair of cyclonic (inside the bay) and anticyclonic (outside the bay) circulations. The satellite-derived SST and chlorophyll images (from MODIS-AQUA satellite) indicate that southward flow along the entrance to the bay has colder surface temperatures than water masses offshore and inside the bay (Figure 2). Also, there is a lower surface chlorophyll concentration in the southward flow than that observed inside the bay. The offshore anticyclonic circulation has warmer and less productive surface water masses in the center of the circulation and relatively more productive water masses at the eastern flank of the circulation (western side of the southward jet). In the bay, there are surface water masses with warmer and higher chlorophyll values along the coast. Satellite images indicate the development of a phytoplankton bloom in the southern part of the bay which extends from Moss Landing, California toward the south.

[18] REMUS surveys on 11 and 12 August (Figure 3) show coincidence of inshore maxima of chlorophyll, BL and backscatter distributions. This suggests that the inshore BL maximum is associated with the planktonic community (dinoflagellates). This conclusion was supported by using general differences in flash kinetics between planktonic dinoflagellates and zooplankton in *Moline et al.* [2009]. The REMUS observations also show a strong BL signal offshore in the deeper water around the M1 mooring location (center of the entrance to the bay) (Figure 3). This deeper offshore BL maximum is below the observed chlorophyll layer. Low values in optical backscatter in the area of the BL maximum (Figure 3) suggest that this observed deeper BL signal is due to larger zooplankton and probably not due to heterotrophic dinoflagellates.

[19] Strong correlations between inshore maxima in chlorophyll, BL and backscatter persists over the next days of REMUS sampling (13–15 August) (Figure 3) and in the DORADO survey on 13 August (going from the M1 mooring to the south of the bay, Figure 4). At the same time, the offshore deep BL signal almost disappeared on 13 August in area around mooring M1 in the REMUS section (Figure 3). The DORADO section also taken on 13 August indicates that the BL maximum is located to the south of the mooring location (Figure 4). This deep offshore BL maximum disappeared on the next day in the DORADO section going through the M1 mooring (Figure 4). The REMUS survey on 15 August (Figure 3) shows a shallow and weak BL signal coinciding with high chlorophyll and backscatter signals around the M1 mooring, which suggests that planktonic dinoflagellates, not zooplankton, might be the source of this weak shallower offshore BL signal on 15 August (Figure 3). This might indicate that with the development of upwelling, offshore water masses with a subsurface layer of bioluminescent zooplankton (observed around the M1 mooring location) were advected southward and replaced with water masses showing relatively high values of chlorophyll fluorescence and backscatter on 15 August. In accordance with HF radar and mooring currents (Figure 1) the presence of phytoplankton in the center of the entrance to the bay might be a result of phytoplankton advection from the northern coast of the bay, due to interaction of the cyclonic eddy in the bay and the strong southward flow along the entrance to the Bay. Because there is a weak BL signal (Figure 3), mostly nonbioluminescent phytoplankton was advected from the north to the mooring M1 location. Surface predictions for 10 and 15 August from the biochemical, physical NCOM ICON model indicate the development of phytoplankton bloom in the southern portion of the bay, which extends from Moss Landing to the south (Figure 5). This is in a good agreement with the satellite-observed phytoplankton bloom on 15 August (Figure 2). The model indicates that one of the reasons for this phytoplankton bloom is an increase of nutrients concentrations (nitrate and silicate) in the southern portion of the bay (Figure 6), where more nutrient-rich water is brought by the southward flow and cyclonic circulation inside the bay. This increase in nutrients together with the sluggish circulation in the southern portion of the bay (Figure 2) provides favorable conditions for the growth of diatoms and small phytoplankton during the development of upwelling.

[20] Between 10 and 15 August, the NCOM ICON model results show the development of a wide, well-defined frontal structure associated with the southward flow along the entrance to the bay (Figure 5). This frontal structure has relatively low surface concentrations of diatoms and zooplankton (in comparison to the bay waters) and a high concentration of small phytoplankton cells in comparison to adjacent bay's water masses to the east and offshore waters masses to the west (Figure 5). Subsurface model results plotted along REMUS section (Figure 7) also indicate a reduction in subsurface diatoms and zooplankton populations in the center of the entrance to the Bay (mooring M1 area) as the upwelling develops. These model predictions are in good agreement with the analysis described above of REMUS and DORADO observations during this period. Observations also show a reduction of zooplankton and the presence of small phytoplankton cells around the M1 mooring location during the upwelling development between 10 and 15 August. As it was discussed above, high values of chlorophyll and backscatter in AUV observations at the M1 mooring location are probably a result of advection of small phytoplankton from the northern part of the bay. Model results support this: between 10 and 15 August, there is a reduction in the model small phytoplankton concentration in the northern area of the bay, and, at the same time, there is an increase in concentration along the entrance to the bay (Figure 5). To further verify these proposed dynamics during the upwelling, we present derivations of an adjoint model to the passive tracer model.

[21] As shown in Appendix A, the adjoint to the passive tracer model (using velocities and diffusivities from the NCOM

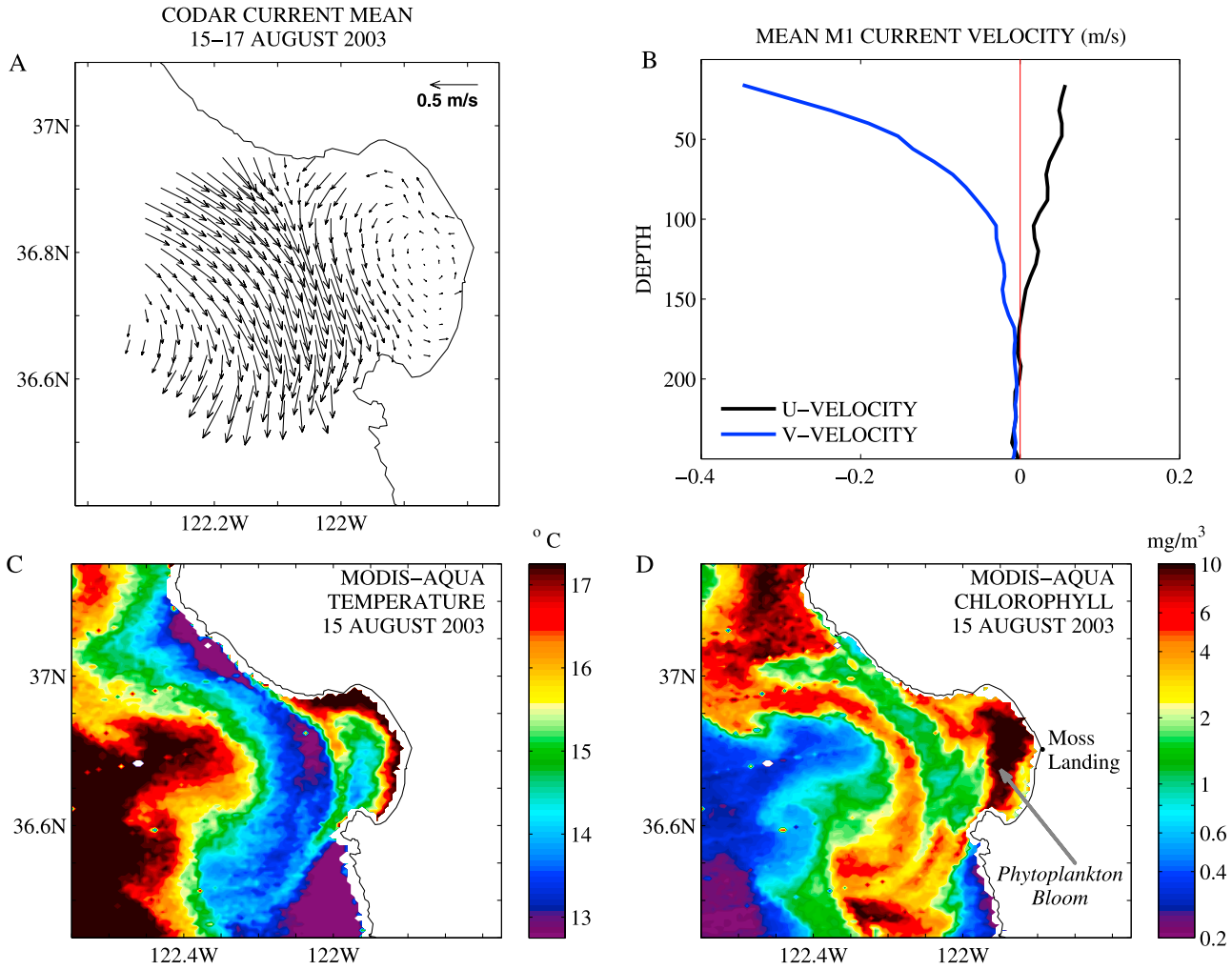

Figure 2. (a) HF radar surface currents averaged over 3 days of upwelling (15–17 August 2003). (b) ADCP observed subsurface profiles of the velocity components at the M1 mooring. Profiles are averaged over 3 days of upwelling. U is the eastward component of velocity, and V is the northward component of velocity. (c) MODIS-AQUA sea surface temperature (SST) and (d) surface chlorophyll on 15 August 2003.

ICON model) shows where the model water masses originate before being circulated to the area of interest [see also *Fukumori et al.*, 2004; *Shulman et al.*, 2010]. In our case, the area of interest is the area around the M1 mooring located in the center of the entrance to the bay. Figure 8 shows the adjoint tracer distributions, which are estimated for volume V in (A2), which consists of 3 by 3 horizontal grids (approximately area of 4 km by 4 km) around the mooring M1 down to a depth of 25 m (the depth to which high chlorophyll and backscatter values were observed on 15 August, see Figure 3). Figure 8 shows vertically integrated adjoint tracer maps at time t equal to 0000 UT 15 August. The adjoint tracer maps are shown for 48, 24, and 11 h prior to the 0000 UT 15 August. In this case, the adjoint passive tracer distributions show areas from which the model tracer-tagged water masses, 48, 24 and 11 h prior to 15 August, were advected and mixed into the target area (around mooring M1). They show that these model water masses mostly originated from the northern part of the bay around 48 and 24 h prior to 15 August, and then mixed with the water masses of the southward flow along the entrance to the bay. This supports the conclusions above regarding phytoplankton and zooplankton dynamics deduced from observations and the biochemical model predictions.

4. Bioluminescence and the Nighttime Water-Leaving Radiance Modeling

[22] *Moline et al.* [2007] proposed an approach for estimating nighttime water-leaving radiance (BLw) due to BL stimulation at depth which used measured Inherent Optical Properties (IOPs) and BL to propagate bioluminescence light from depth to surface. However, the *Moline et al.* [2007] methodology does not provide the capability to forecast the nighttime water-leaving radiance on time scales 1–5 days (only under assumption of persistence of observed conditions). Forecasting models of bioluminescence intensity (as for example proposed by *Shulman et al.* [2003,

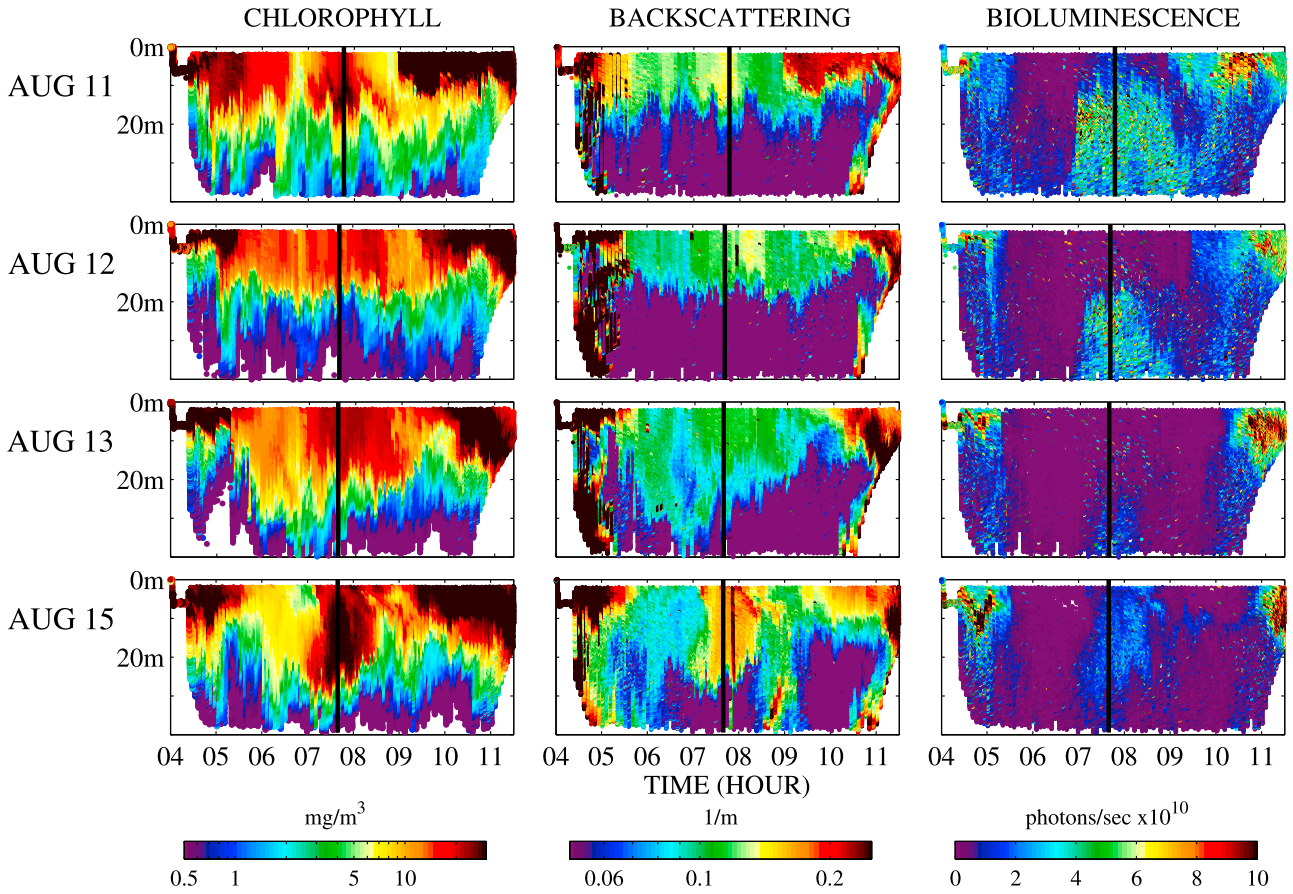

Figure 3. AUV REMUS observed chlorophyll, backscattering, and bioluminescence during 11–15 August. Solid vertical lines indicate location of the M1 mooring.

2005]), as well as forecasting models of IOPs properties of the water column are needed.

[23] In the present study, the BL model described in section 2.2 is initialized on 14 August by using BL data from four AUVs sections: DORADO sections taken 13 and 14 August, and AUV REMUS sections taken on 14 August (Figure 1). The initialization procedure is described in detail by *Shulman et al.* [2003, 2005]. After initialization, the BL

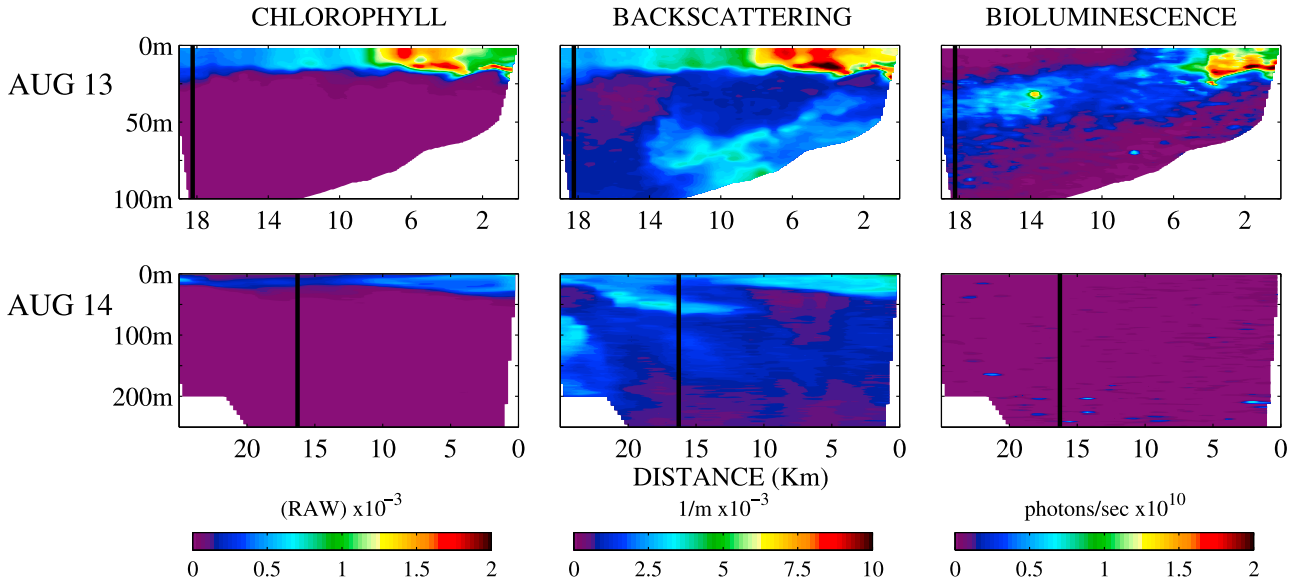

Figure 4. AUV DORADO observed chlorophyll, backscattering, and bioluminescence on 13 and 14 August.

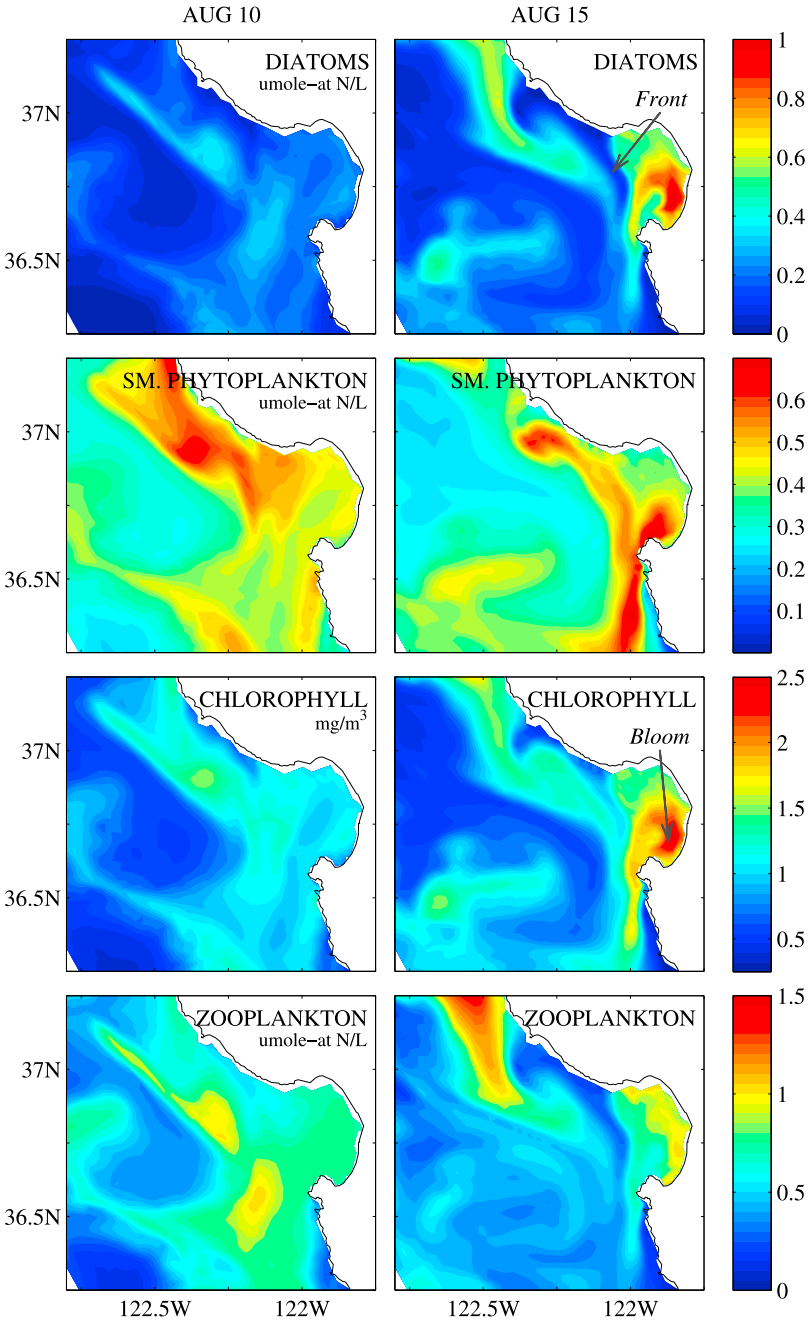

Figure 5. Surface predictions for 10 and 15 August from the coupled biochemical, physical NCOM ICON model.

dynamics are predicted forward in time by using the advection-diffusion-reaction model. Figure 9 shows surface and subsurface predictions of BL intensity on 15 August (1 day later after the model initialization, values are normalized by 10^9 photons/s). The predicted BL distributions in the Bay are in good agreement with the above analysis of BL observations and the biochemical, physical NCOM ICON model predictions. There are high levels of inshore modeled BL (Figure 9), which correlate with the observed BL maxima and high concentrations of chlorophyll. At the same time, the biggest differences with observations are in BL distributions along the entrance to the bay and offshore. The model BL shows high values along the entrance to the bay (along the frontal structure discussed in the biochemical model predictions). However, as it was discussed above, observations show a very weak BL signal in the area around the M1 mooring location on 15 August. It is clear that the high value of model BL are a result of the advection by the southward flow of BL intensity from the northern part of the bay. However, this advection of bioluminescent phytoplankton did not happen in reality as illustrated in section 3. Why were bioluminescent dinoflagellates not advected by the southward flow? In accordance with the biochemical model (Figure 6), nutrients were in abundance along the entrance to the bay (carried by the southward flow). At the same time, the entrance to the bay has very strong currents,

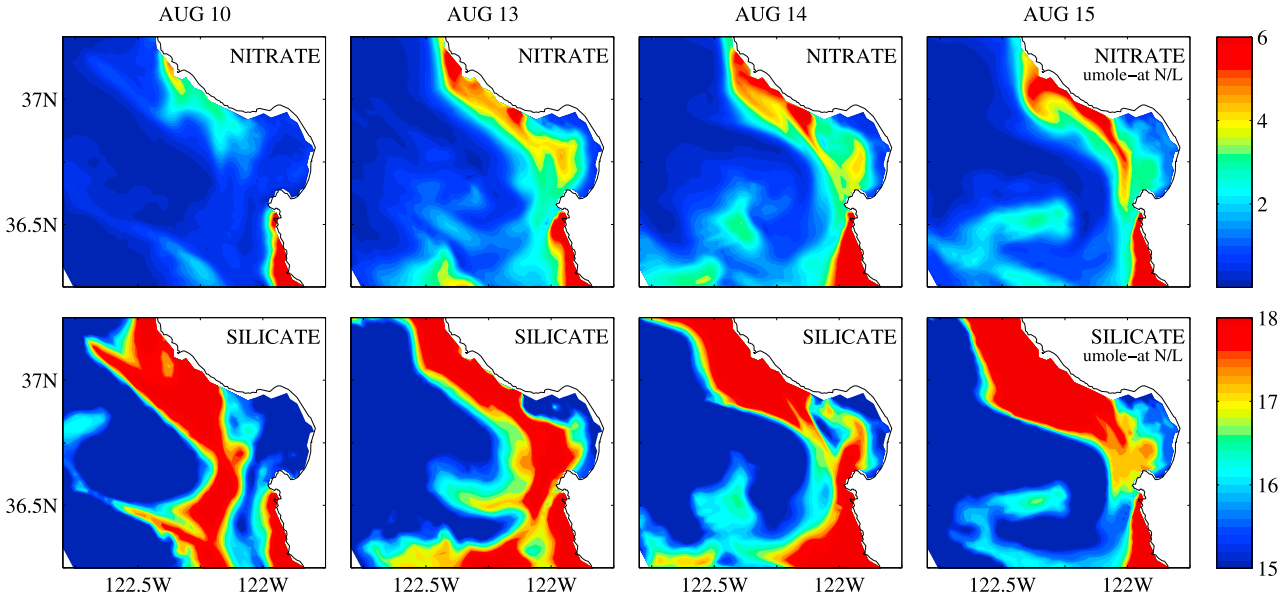

Figure 6. Surface predictions of nitrate and silicate from the coupled biochemical, physical NCOM ICON model.

which create unfavorable conditions for growth and survival of dinoflagellates [*Jones and Gowen*, 1990]. This suggests that advective and diffusive processes alone cannot explain many observed features of spatial and temporal variability of the BL intensity. Modeling of behavioral dynamics of bioluminescent organisms, as well as modeling of sources and sink terms representing ecological interactions controlling the bioluminescence [*Benoit-Bird et al.*, 2010; *Jones and Gowen*, 1990], should be added to BL modeling methodology in the future.

[24] Dynamical, predictive biochemical and bioluminescence intensity models provide the possibility to model and forecast the nighttime water-leaving radiances due to stimulation of BL at depth. We used the constituents from the NCOM ICON biochemical model to estimate IOPs (absorption and backscattering) based on the methodology outlined by *Fujii et al.* [2007].

[25] If the intensity of the light from the stimulated BL and IOPs are known, the propagation of the light to the surface can be estimated with the radiative transfer models like Hydrolight or a reduced version of Hydrolight-Ecolight model [*Mobley and Sundman*, 2001a, 2001b]. However, in both cases, the use of these models with the coupled, biochemical, physical, nested, data assimilative models are computationally expensive. In the present study we estimated the propagation of light from the BL source to the surface by inverting the *Penta et al.* [2008] scheme which is used in the biochemical model for attenuating the PAR with the depth (see section 2.2).

[26] Figure 10 (right) shows water-leaving radiance (BLw) at the surface due to stimulation of the modeled BL intensity over the entire model domain at different depths (5, 15, and 25 m) on 15 August. The modeled BL 3-D distributions (normalized by 10^9) are shown in Figure 10 (middle) for different depths of stimulations (see also Figure 9 and above discussions about the BL model results on 15 August). Figure 10 (left) shows a sum of a (absorption) and b_b (backscattering) averaged from the depth of BL stimulation to the surface. Values of a and b_b are estimated from the biochemical model in accordance with *Fujii et al.* [2007].

[27] There are high values of estimated water-leaving radiance in the areas close to the coast (Figure 10), which correlates with observed and model predicted BL maxima along the coastline. At the same time, Figure 10 also shows high values of water-leaving radiances along the entrance to the bay (along the frontal structure discussed above), which is probably an artificial feature due to above discussed differences between modeled and observed BL distributions along the entrance to the bay. The model-predicted artificially strong BL signal is illuminated in the surface and subsurface by the relatively lower values of IOPs along the entrance to the bay (Figure 10). These low IOP values are associated with the development of the frontal structure with relatively (to the bay and offshore) clear water masses of the southward flowing jet (Figures 2 and 5).

5. Conclusions

[28] Observations of physical, bio-optical properties (including bioluminescence) together with results from dynamical biochemical, physical (NCOM ICON) and bioluminescence models are used to interpret the development of the upwelling event during August 2003 AOSN II field experiment.

[29] Satellite observations and the NCOM ICON model show the development of the phytoplankton bloom in the southern portion of Monterey Bay. The model results suggest that one of the reasons for development of this phytoplankton bloom is the increase of nutrients concentrations (nitrate and silicate) in the southern portion of the Bay where nutrient-rich water masses are brought in by the southward flow and cyclonic circulation inside the Bay. This increase in nutrients together with the sluggish circulation in the southern portion of the Bay provides favorable conditions for the phytoplankton growth.

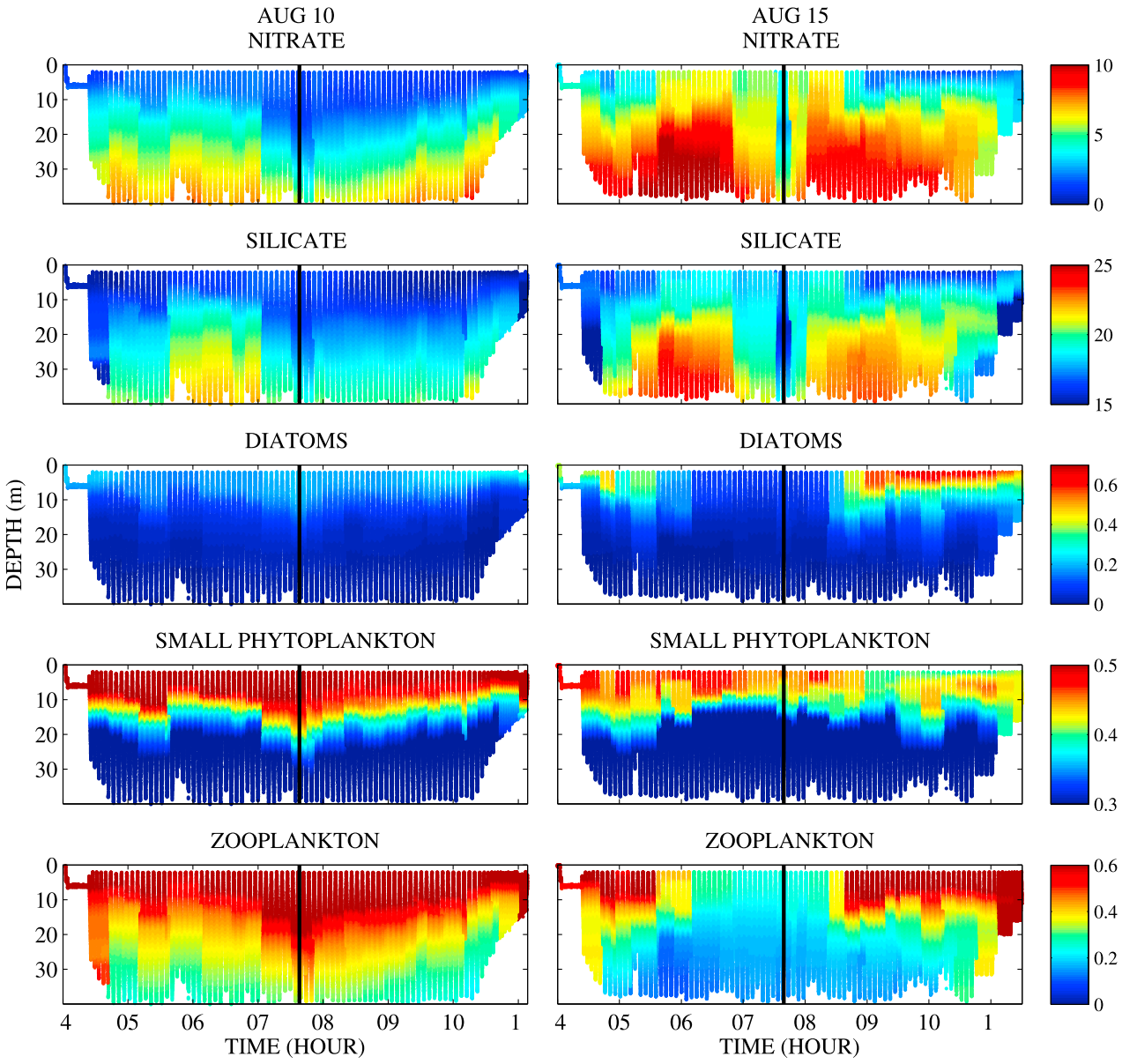

Figure 7. Subsurface model predictions along the REMUS transect on 10 and 15 August. Solid vertical lines indicate location of the M1 mooring.

[30] Inshore AUV observations show consistent coincidence of chlorophyll, backscatter, and bioluminescence maxima during upwelling development. Offshore AUV observations (taken at the entrance to the Bay) show deeper bioluminescence maxima below the surface layers of high chlorophyll and backscatter values during the earlier stage of the upwelling development. These observations lead to the conclusion that inshore bioluminescence maxima are associated with the phytoplankton (dinoflagellates), while offshore BL maxima are due to larger zooplankton which is in agreement with general differences in flash kinetics between planktonic dinoflagellates and zooplankton presented by *Moline et al.* [2009]. The observed deep offshore BL maximum disappeared during the upwelling development and became a shallower and much weaker signal coinciding with high chlorophyll and backscatter values offshore. Observations together with results from the NCOM ICON model and distributions of the passive tracer adjoint model suggest that with the development of upwelling, the offshore water masses with the subsurface layer of bioluminescent zooplankton were advected southward and replaced with water masses showing relatively high values of chlorophyll fluorescence and backscatter. This high presence of the phytoplankton at the entrance to the bay is a result of its advection from the northern coast of the bay by the strong southward flow. Because there is a weak observed BL signal, mostly nonbioluminescent phytoplankton was advected from the north.

[31] Results from the dynamical bioluminescence model show agreement with the observed inshore BL observations. At the same time, the model shows high values of BL intensity along the entrance to the bay (along the path of the

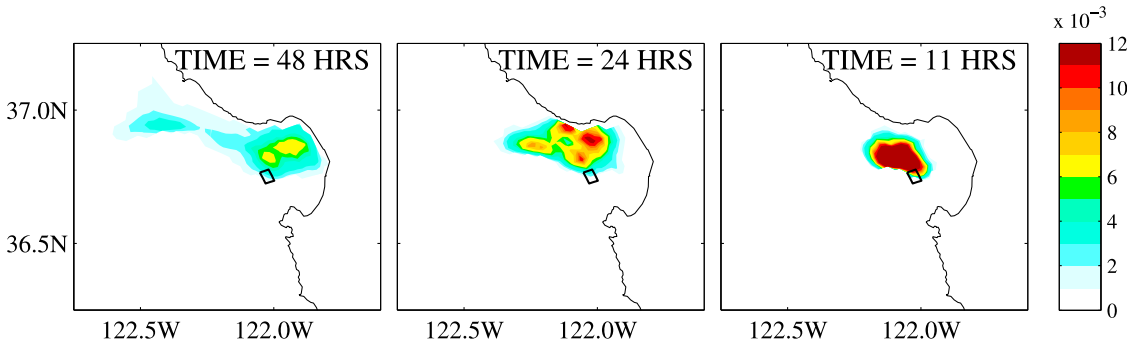

Figure 8. Adjoint passive tracer distributions on 15 August.

southward flow); while observations show that bioluminescent dinoflagellates mostly escaped the southward advection from the northern part of the bay. This indicates that the BL modeling approach (which is based on advective and diffusive processes) should include the modeling of behavioral dynamics of bioluminescent organisms, as well as the modeling of sources and sink terms, representing ecological interactions controlling the bioluminescence.

[32] The biochemical and bioluminescence models presented in this study are combined into a methodology for estimating the nighttime water-leaving radiance due to stimulated bioluminescence. The results show high values of estimated water-leaving radiance in areas along the coastline, where high values of BL were observed and model predicted. At the same time, estimated water-leaving radiances have high offshore values (along the entrance to the Bay), which

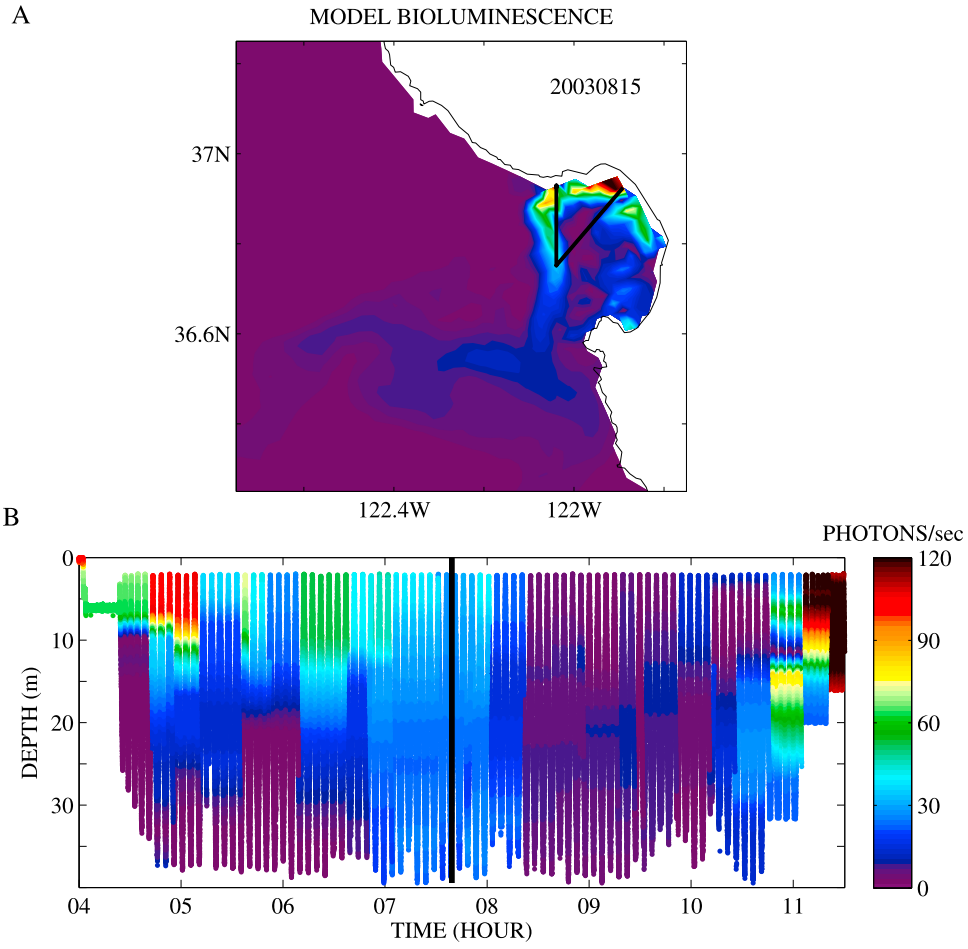

Figure 9. (a) Surface and (b) subsurface (along the REMUS transect) model-predicted BL distributions. Solid vertical line indicates location of the M1 mooring.

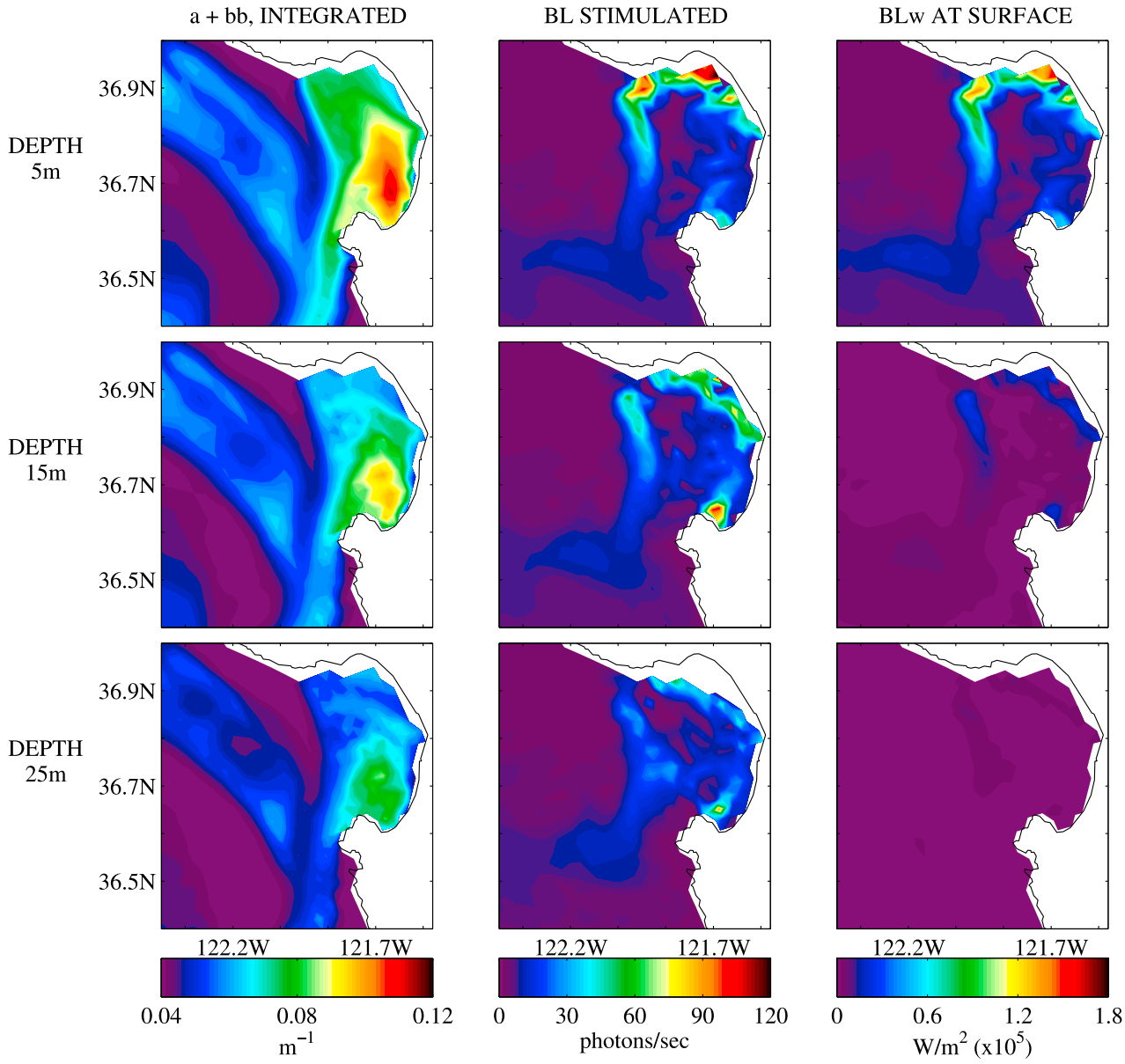

Figure 10. (right) Water-leaving radiance at the surface due to stimulation of the modeled BL intensity at different depths (5, 15, and 2 5m) on 15 August. (middle) The modeled BL intensity for different depths of stimulations, and (left) a sum of a (absorption) and b_b (backscattering) averaged from the depth of BL stimulation to the surface.

are comparable to the coastal distributions. These offshore high values of water-leaving radiance are a result of artificial, model-predicted BL maximum along the entrance to the Bay.

Appendix A: Passive Tracer and Its Adjoint

[33] Consider the passive tracer equation for concentration C(x, y, z, t)

$$\frac{\partial C}{\partial t} = -u\frac{\partial C}{\partial x} - v\frac{\partial C}{\partial y} - w\frac{\partial C}{\partial z} + \frac{\partial}{\partial x}\left(A\frac{\partial C}{\partial x}\right) + \frac{\partial}{\partial y}\left(A\frac{\partial C}{\partial y}\right) + \frac{\partial}{\partial z}\left(K\frac{\partial C}{\partial z}\right). \quad \text{(A1)}$$

With initial conditions at time $t = t_0$

$$C = C_0,$$

where diffusivities (A and K) and velocities (u,v,w) are from the NCOM ICON model described in section 2.2.

[34] Let us consider the following objective function J at time $t > t_0$

$$J = \frac{\int_V C(\tau, t)\,d\tau}{\int_V d\tau}, \quad \text{(A2)}$$

where V is a particular subdomain (target area) of the modeling domain, τ is the location in the model domain with coordinates (x,y,z), and $d\tau$ is a volume element. Therefore, function J is the normalized content of tracer C in the domain V at time t.

[35] By using the adjoint for the tracer equation (A1), the gradient of the function J (equation (A2)) at time t with respect to the initial concentration C_0 at time t_0, can be estimated

$$s = \frac{\partial J}{\partial C_0}, \tag{A3}$$

where s is the sensitivity, $\frac{\partial J}{\partial C_0}$ is the gradient of J (at time t) with respect to initial conditions C_0. Sensitivity, s, is a function of x, y, z and times, t_0 and t, and can be estimated by seeding the adjoint variable with a unit value at each grid point in the volume V at time t, and integrating the adjoint of the tracer model backward in time to time t_0 [*Fukumori et al.*, 2004; *Shulman et al.*, 2010]. The function s(x, y, z, t) is called the adjoint tracer sensitivity, as well as the adjoint tracer distribution (because the function s, is the result of the adjoint tracer model integration).

[36] Lets introduce some finite perturbation ΔC_0 at location $X_0 = \{x_0, y_0, z_0\}$ to the initial concentration C_0 at time t_0, according to (A3) we would have

$$\Delta J = s(x_0, y_0, z_0, t_0, t) \cdot \Delta C_0. \tag{A4}$$

According to (A2) and (A4), the adjoint tracer distribution $s(x_0, y_0, z_0, t_0, t)$ represents a fraction of tracer ΔC_0, which makes its way to the volume V from time t_0 to time t. Due to the linearity of the passive tracer and its adjoint problems, the adjoint tracer distribution $s(x, y, z, t_0, t)$ will represent the fraction of the tracer-tagged water that makes its way from location (x, y, z) at time t_0 to the volume V at time t [see also *Fukumori et al.*, 2004]. Therefore, the adjoint tracer distribution provides information on the model tracer history and identifies origin and pathways of the model tracer-tagged water masses in the past, which circulated into the target area, and therefore contain useful information about model circulation patterns and the propagation of information within the system.

[37] **Acknowledgments.** This research was funded through the Naval Research Laboratory (NRL) project, "Bio-optical Studies of Predictability and Assimilation in the Coastal Environment" under program element 61153N and grants N0001409WX20966, N0001410WX20482, N0001409AF00002, and N0001410AF00002, sponsored by the Office of Naval Research, Marine Mammals and Biology Program. We are grateful to the whole AOSN team for discussions and their collaborations. We thank Jeff Paduan of NPS for collaborations on HF radar surface currents and Dmitri Nechaev of USM for helpful discussions about adjoint. Our thanks also go to Fei Chai and Lei Shi of UMaine for help with the biochemical model. Mooring data were provided by Francisco Chavez of MBARI. We thank Peter Sakalaukus of USM for programming and computer support. Computer time for the numerical simulations was provided through a grant from the Department of Defense High Performance Computing Initiative. This manuscript is NRL contribution 7330-10-398.

References

Barron, C. N., A. B. Kara, H. E. Hurlburt, C. Rowley, and L. F. Smedstad (2004), Sea surface height predictions from the global Navy Coastal Ocean Model (NCOM) during 1998–2001, *J. Atmos. Oceanic Technol.*, *21*, 1876–1893, doi:10.1175/JTECH-1680.1.

Benoit-Bird, K. J., M. A. Moline, C. M. Waluk, and I. C. Robbins (2010), Integrated measurements of acoustical and optical thin layers, part I: Vertical scales of association, *Cont. Shelf Res.*, *30*, 17–28, doi:10.1016/j.csr.2009.08.001.

Chai, F., R. C. Dugdale, T.-H. Peng, F. P. Wilkerson, and R. T. Barber (2002), One-dimensional ecosystem model of the equatorial Pacific upwelling system. Part I: Model development and silicon and nitrogen cycle, *Deep Sea Res. Part II*, *49*, 2713–2745, doi:10.1016/S0967-0645(02)00055-3.

Cummings, J. A. (2005), Operational multivariate ocean data assimilation, *Q. J. R. Meteorol. Soc.*, *131*, 3583–3604, doi:10.1256/qj.05.105.

Doyle, J. D., Q. Jiang, Y. Chao, and J. Farrara (2009), High-resolution real-time modeling of the marine atmospheric boundary layer in support of the AOSN-II field campaign, *Deep Sea Res. Part II*, *56*, 87–99.

Fox, D. N., C. N. Barron, M. R. Carnes, M. Booda, G. Peggion, and J. Van Gurley (2002), The Modular Ocean Data Assimilation System, *Oceanography*, *15*, 22–28.

Fujii, M., E. Boss, and F. Chai (2007), The value of adding optics to ecosystem models: A case study, *Biogeosciences*, *4*, 817–835, doi:10.5194/bg-4-817-2007.

Fukumori, I., T. Lee, B. Cheng, and D. Menemenlis (2004), The origin, pathway, and destination of Niño-3 water estimated by a simulated passive tracer and its adjoint, *J. Phys. Oceanogr.*, *34*, 582–604, doi:10.1175/2515.1.

Haddock, S. H. D., M. A. Moline, and J. F. Case (2010), Bioluminescence in the sea, *Annu. Rev. Mar. Sci.*, *2*, 443–493.

Herren, C. M., S. H. D. Haddock, C. Johnson, M. A. Moline, and J. F. Case (2005), A multi-platform bathyphotometer for fine-scale, coastal bioluminescence research, *Limnol. Oceanogr. Methods*, *3*, 247–262.

Jones, K. J., and R. J. Gowen (1990), Influence of stratification and irradiance regime on summer phytoplankton composition in coastal and shelf seas of the British Isles, *Estuarine Coastal Shelf Sci.*, *30*(6), 557–567, doi:10.1016/0272-7714(90)90092-6.

Martin, P. J. (2000), Description of the Navy Coastal Ocean Model version 1.0, *Rep. NRL/FR/732-00—9962*, Nav. Res. Lab., Stennis Space Center, Miss.

Mobley, C. D., and L. K. Sundman (2001a), HydroLight 4.2 users' guide, report, Sequoia Sci., Inc., Mercer Island, Wash. (Available at http://www.HydroLight.info).

Mobley, C. D., and L. K. Sundman (2001b), HydroLight 4.2 technical documentation, report, Sequoia Sci., Inc., Mercer Island, Wash. (Available at http://www.HydroLight.info).

Moline, M. A., S. M. Blackwell, B. Allen, T. Austin, N. Forrester, R. Goldsborogh, M. Purcell, R. Stokey, and C. vonAlt (2005), Remote Environmental Monitoring Units (REMUS): An autonomous vehicle for characterizing coastal environments, *J. Atmos. Oceanic Technol.*, *22*, 1797–1808, doi:10.1175/JTECH1809.1.

Moline, M. A., M. J. Oliver, C. D. Mobley, L. Sundman, T. Bensky, T. Bergmann, W. P. Bissett, J. Case, E. H. Raymond, and O. M. E. Schofield (2007), Bioluminescence in a complex coastal environment: 1. Temporal dynamics of nighttime water-leaving radiance, *J. Geophys. Res.*, *112*, C11016, doi:10.1029/2007JC004138.

Moline, M. A., S. M. Blackwell, J. F. Case, S. H. D. Haddock, C. M. Herren, C. M. Orrico, and E. Terrill (2009), Bioluminescence to reveal structure and interaction of coastal planktonic communities, *Deep Sea Res. Part II*, *56*, 232–245, doi:10.1016/j.dsr2.2008.08.002.

Paduan, J. D., and I. Shulman (2004), HF radar data assimilation in the Monterey Bay area, *J. Geophys. Res.*, *109*, C07S09, doi:10.1029/2003JC001949.

Pennington, J. T., and F. P. Chavez (2000), Seasonal fluctuations of temperature, salinity, nitrate, chlorophyll and primary production at station H3/M1 over 1989–1996 in Monterey Bay, California, *Deep Sea Res. Part II*, *47*, 947–973, doi:10.1016/S0967-0645(99)00132-0.

Penta, B., Z. Lee, R. Kudela, S. Palacios, D. Gray, J. Jolliff, and I. Shulman (2008), An underwater light attenuation scheme for marine ecosystem models, *Opt. Express*, *16*, 16,581–16,591.

Ramp, S. R., et al. (2009), The Autonomous Ocean Sensing Network (AOSN) predictive skill experiment in the Monterey Bay, *Deep Sea Res. Part II*, *56*, 8–26.

Rhodes, R. C., et al. (2002), Navy real-time global modeling systems, *Oceanography*, *15*, 29–43.

Rosenfeld, L. K., F. B. Schwing, N. Garfield, and D. E. Tracy (1994), Bifurcated flow from an upwelling center: A cold water source for Monterey Bay, *Cont. Shelf Res.*, *14*, 931–964, doi:10.1016/0278-4343(94)90058-2.

Rosmond, T. E., J. Teixeira, M. Peng, T. F. Hogan, and R. Pauley (2002), Navy Operational Global Atmospheric Prediction System (NOGAPS): Forcing for ocean models, *Oceanography*, *15*, 99–108.

Ryan, J. P., H. M. Dierssen, R. M. Kudela, C. A. Scholin, K. S. Johnson, J. M. Sullivan, A. M. Fischer, E. V. Rienecker, P. R. McEnaney, and

F. P. Chavez (2005), Coastal ocean physics and red tides: An example from Monterey Bay, California, *Oceanography*, *18*, 246–255.

Shulman, I., S. H. D. Haddock, D. J. McGillicuddy, J. D. Paduan, and W. P. Bissett (2003), Numerical modeling of bioluminescence distributions in the coastal ocean, *J. Atmos. Oceanic Technol.*, *20*, 1060–1068, doi:10.1175/1468.1.

Shulman, I., D. J. McGillicuddy Jr., M. A. Moline, S. H. D. Haddock, J. C. Kindle, D. Nechaev, and M. W. Phelps (2005), Bioluminescence intensity modeling and sampling strategy optimization, *J. Atmos. Oceanic Technol.*, *22*, 1267–1281, doi:10.1175/JTECH1760.1.

Shulman, I., J. Kindle, P. Martin, S. deRada, J. Doyle, B. Penta, S. Anderson, F. Chavez, J. Paduan, and S. Ramp (2007), Modeling of upwelling/relaxation events with the Navy Coastal Ocean Model, *J. Geophys. Res.*, *112*, C06023, doi:10.1029/2006JC003946.

Shulman, I., et al. (2009), Impact of glider data assimilation on the Monterey Bay model, *Deep Sea Res. Part II*, *56*, 128–138.

Shulman, I., S. Anderson, C. Rowley, S. deRada, J. Doyle, and S. Ramp (2010), Comparisons of upwelling and relaxation events in the Monterey Bay area, *J. Geophys. Res.*, *115*, C06016, doi:10.1029/2009JC005483.

S. Anderson, B. Penta, and I. Shulman, Oceanography Division, Naval Research Laboratory, Bldg. 1009, Stennis Space Center, MS 39529, USA. (igor.shulman@nrlssc.navy.mil)

S. H. D. Haddock, Monterey Bay Aquarium Research Institute, 7700 Sandholdt Rd., Moss Landing, CA 95039, USA.

M. A. Moline, Center for Marine and Coastal Sciences, Biological Sciences Department, California Polytechnic State University, San Luis Obispo, CA 93407, USA.

M. Oliver, College of Marine and Earth Sciences, University of Delaware, 700 Pilottown Rd., Lewes, DE 19958, USA.